Supporting Information

Ongoing anthropogenic eutrophication of the catchment area threatens the Doñana World Heritage Site (South-west Spain)

Irene Paredes[1*], Francisco Ramírez[2], David Aragonés[3], Miguel Ángel Bravo[4], Manuela G. Forero[5], Andy J. Green[1]

[1]Department of Wetland Ecology, Estación Biológica de Doñana (CSIC), Avda. Américo Vespucio 26, 41092 Sevilla, Spain.

[2]Departament de Biologia Evolutiva, Ecologia i Ciències Ambientals, Universitat de Barcelona, Av. Diagonal 643, 08028, Barcelona, Spain.

[3]Remote Sensing and GIS Laboratory (LAST-EBD), Estación Biológica de Doñana (CSIC), Avda. Américo Vespucio 26, 41092 Sevilla, Spain

[4]Monitoring Team on Natural Resources and Processes, Estación Biológica de Doñana (CSIC), Avda. Américo Vespucio 26, 41092 Sevilla, Spain

[5]Department of Conservation Biology, Estación Biológica de Doñana (CSIC), Avda. Américo Vespucio 26, 41092 Sevilla, Spain.

*corresponding author: irene.paredeslosada@gmail.com (I. Paredes)

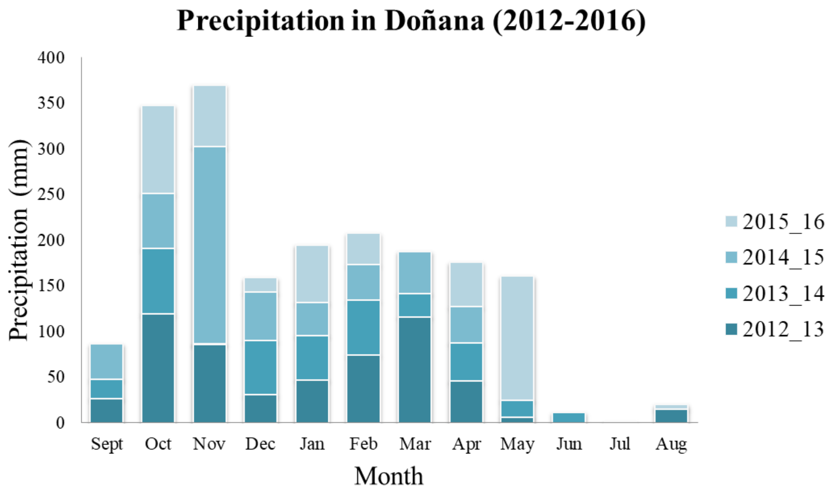

Figure S1. Monthly precipitation in Doñana National Park (DNP) over the four consecutive hydrological years included in this study. Each hydrological year extends from September until the following August. Data were collected from the Meteorological Station located at "El Palacio" within DNP.

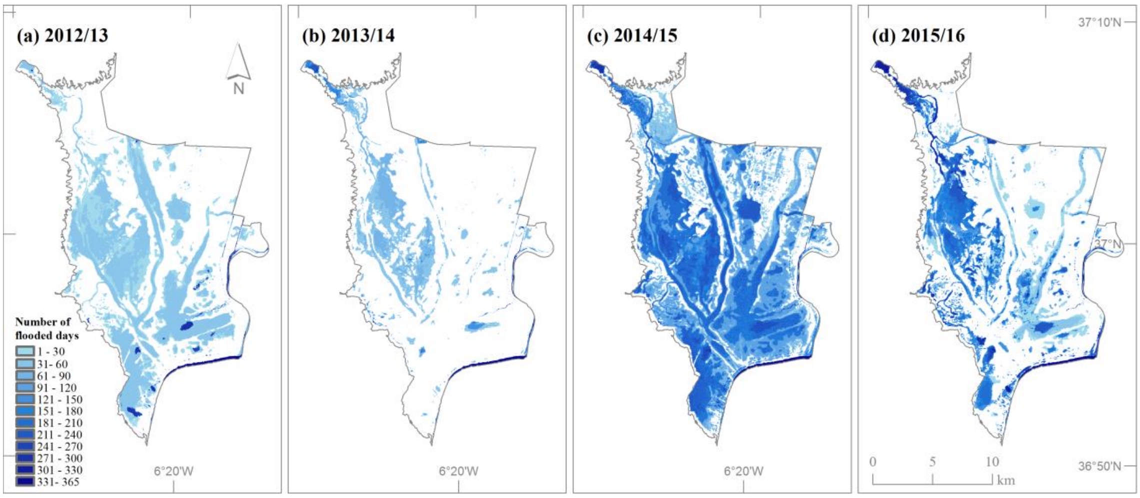

Figure S2. Estimated hydroperiod for the hydrological years 2012/13 (total precipitation=566 mm), 2013/14 (359 mm), 2014/15 (528 mm) and 2015/16 (469 mm). Colour intensity indicates the number of days each pixel was detected as flooded according to inundation masks from Landsat images (see Díaz-Delgado et *al.* 2016 for methodological details).

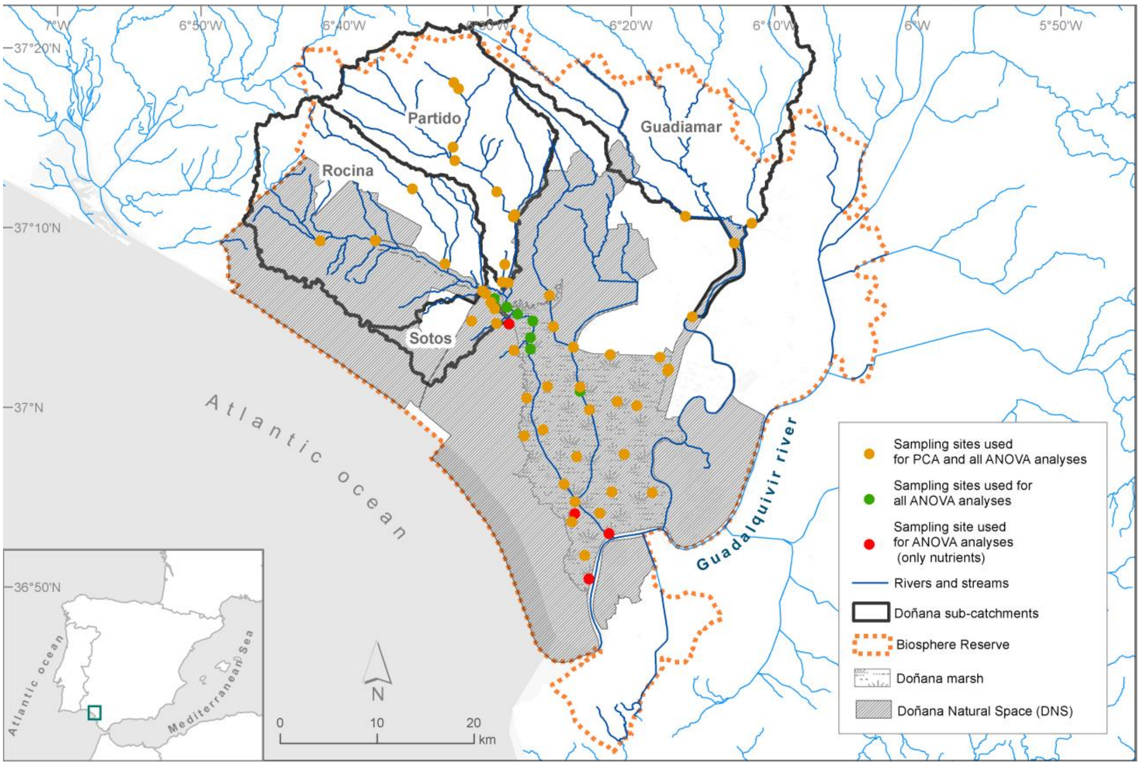

Figure S3. Location of sampling points used in the PCA analysis (n_{sites}=49; $n_{samples}$=338; orange dots), the two-way ANOVA analyses of nutrient concentrations (n_{sites}=59; $n_{samples}$=434; orange, green and red dots) and the ANOVA analyses of chla (n_{sites}=55; $n_{samples}$=264; orange and green dots). Data were collected between January 2013 and June 2016.

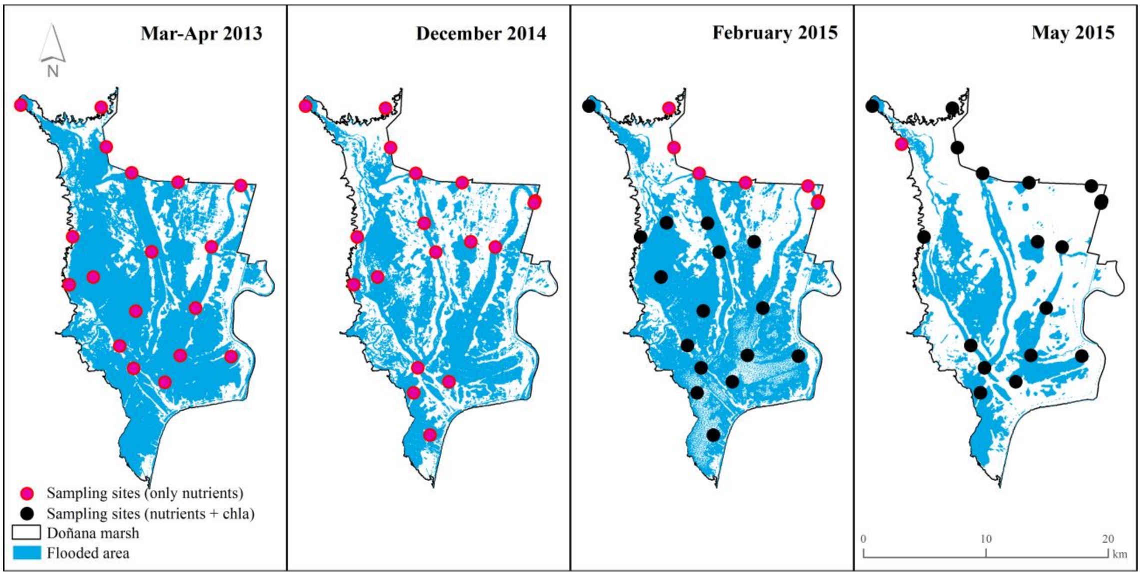

Figure S4. Location of sampling points within the Doñana marsh from which we obtained the nutrient (pink and black dots) and chla (only black dots) data used to perform linear regression models over the four sampling periods with the highest flooding level during our entire study period. Inundation masks represent the flooded area for the following dates: 19/04/2013, 10/12/2014, 28/02/2015 and 11/05/2015.

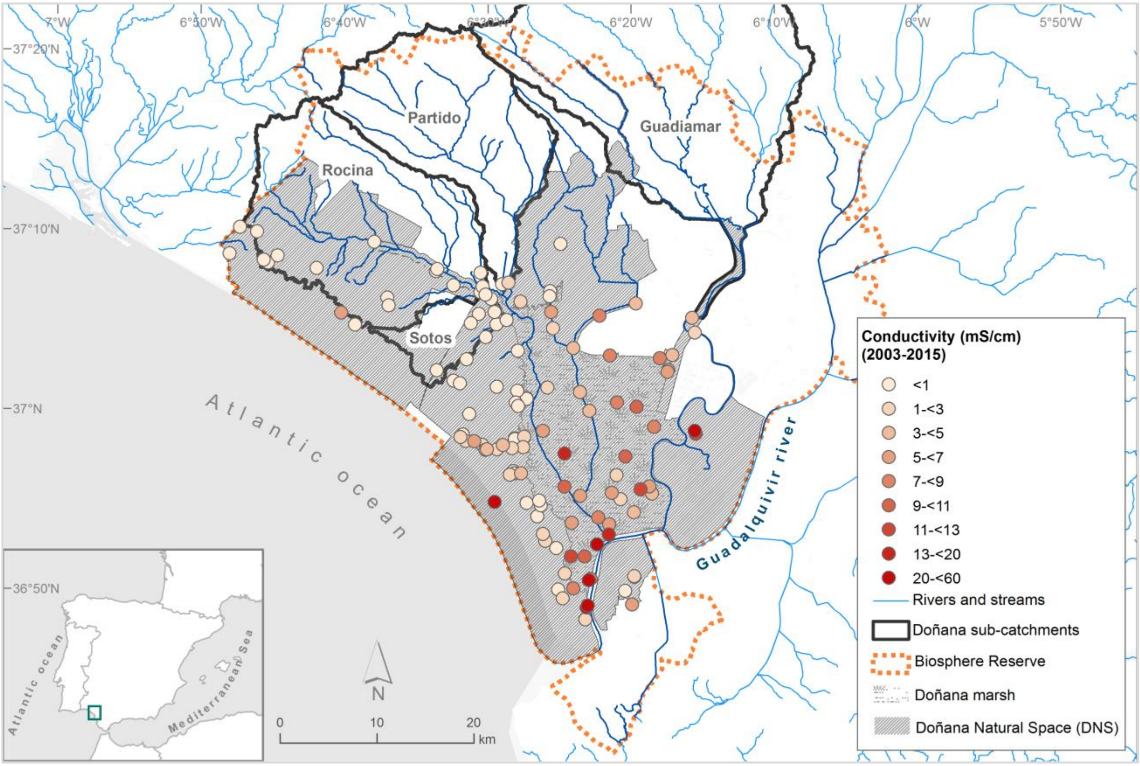

Figure S5. Conductivity (mS cm^{-1}) gradient across Doñana Natural Space (shaded area). Dots represent mean conductivity values of all samples collected at each point between 1st April and 30th June during the period 2003 to 2015. These data were collected by the Monitoring Team for Natural Resources and Processes of the Doñana Biological Station using a WTW (Weilheim, Germany) Multi-340i handheld meter for *in situ* measurements. Many of these points were not used in our own study (e.g. those in dune ponds).

Table S1. Summary of conductivity, depth and stable isotope data collected between January 2013 and June 2016 in the marsh and the three streams.

	Waterbody			
Variables	**Partido (n= 92)**	**Rocina/Sotos (n= 79)**	**Guadiamar (n= 33)**	**Marsh (n= 137)**
Cond (μS cm^{-1})				
Min.	267	222	325	156
1st Qu.	945	393.5	719	1070
Median	1162	553	1439	2460
Mean ± s.d.	1191 ± 766.4	544.2 ± 195.8	2114 ±1908.2	4330 ± 5737.12
3rd Qu.	1317	626	2690	5090
Max.	7860	1270	7820	32900
Depth (cm)				
Min.	1	5	5	1
1st Qu.	15	10	26	15
Median	23	20	60	28
Mean ± s.d.	36.2 ± 52.7	26.8 ± 23.8	67.6 ± 59.2	31± 22.1
3rd Qu.	40	35	100	42
Max.	480	130	300	150
δ^2H (‰)				
Min.	-50.1	-55.9	-49	-52
1st Qu.	-28	-29.3	-35.6	-21.5
Median	-25.7	-25.8	-24.3	-1.3
Mean ± s.d.	-26.9 ± 5.5	-26.5 ± 7.3	-23.8 ± 13.9	-1.5 ± 25.9
3rd Qu.	-23.9	-23.1	-14.9	13.1
Max.	-17.9	-3.4	7.5	68.2

Table S2. Two-way analysis of variance (two-way ANOVA) with nutrient and chlorophyll-*a* (chla) concentrations as dependent variables (all log-transformed), and waterbody as categorical predictor. Coefficients for waterbody 'Marsh' are not shown because they are aliased, but they are effectively zero. 'Sampling period' refers to 16 different field campaigns carried out between January 2013 and May 2016. The degrees of freedom of the residuals were 411 for all nutrient effects and 250 for chla. This table corresponds to Fig. 9 in the manuscript.

Variable	Effect	Level of effect	Estimate ± S.E.	Df	F	P	Model parameters	
	Intercept		-3.92 ± 0.40	1	96.51	<0.0001		
		Guadiamar	0.92 ± 0.36				**Adj. R^2**	0.42
Log PO4	Waterbody	Rocina/Sotos	1.82 ± 0.28	3	50.03	<0.0001	**F**	18.36
		Partido	3.70 ± 0.30				**P**	<0.0001
	Sampling period			15	12.02	<0.0001		
	Intercept		-1.92 ± 0.15	1	155.65	<0.0001		
		Guadiamar	0.38 ± 0.13				**Adj. R^2**	0.49
Log TP	Waterbody	Rocina/Sotos	1.04 ± 0.10	3	81.69	<0.0001	**F**	24.16
		Partido	1.80 ± 0.11				**P**	<0.0001
	Sampling period			15	12.65	<0.0001		
	Intercept		-3.34 ± 0.57	1	34.00	<0.0001		
		Guadiamar	0.79 ± 0.51				**Adj. R^2**	0.20
Log NH4	Waterbody	Rocina/Sotos	0.14 ± 0.40	3	25.44	<0.0001	**F**	7.18
		Partido	3.31 ± 0.43				**P**	<0.0001
	Sampling period			15	3.53	<0.0001		
	Intercept		-6.63 ± 0.73	1	82.50	<0.0001		
		Guadiamar	5.31 ± 0.66				**Adj. R^2**	0.53
Log NO3	Waterbody	Rocina/Sotos	6.49 ± 0.52	3	97.11	<0.0001	**F**	28.70
		Partido	9.08 ± 0.55				**P**	<0.0001
	Sampling period			15	15.02	<0.0001		
	Intercept		-5.58 ± 0.31	1	319.59	<0.0001		
		Guadiamar	1.4 ± 0.28				**Adj. R^2**	0.50
Log NO2	Waterbody	Rocina/Sotos	1.75 ± 0.22	3	92.92	<0.0001	**F**	25.54
		Partido	3.95 ± 0.23				**P**	<0.0001
	Sampling period			15	12.06	<0.0001		
	Intercept		1.09 ± 0.10	1	117.31	<0.0001		
		Guadiamar	0.04 ± 0.09				**Adj. R^2**	0.52
Log TN	Waterbody	Rocina/Sotos	0.49 ± 0.07	3	97.11	<0.0001	**F**	27.87
		Partido	1.26 ± 0.07				**P**	<0.0001
	Sampling period			15	14.02	<0.0001		
	Intercept		-5.57 ± 0.18	1	968.27	<0.0001		
		Guadiamar	1.04 ± 0.26				**Adj. R^2**	0.14
Log Chla	Waterbody	Rocina/Sotos	0.54 ± 0.18	3	8.87	<0.0001	**F**	4.54
		Partido	0.02 ± 0.19				**P**	<0.0001
	Sampling period			10	3.24	<0.0001		

Table S3. Surface water flow (m^3s^{-1}) measured at different sites of the Rocina and Partido streams during February, April and May in 2016. We used a handheld Acoustic Doppler Velocimeter (Sontek FlowTracker). Final flow value is the average of several measurements along a transversal transect of the stream.

	Surface water flow (m^3s^{-1}) [mean velocity ($m\ s^{-1}$)]			
Stream sites	**25th Feb. 2016**	**10th April 2016**	**20th, †21st April 2016**	**24th, ††25th May 2016**
Rocina stream – upstream (*Ortigas bridge*)	0.0079 [0.1156]	0.0048 [0.0732]	0.1898 [0.3594]	0.0141[0.1652]
Rocina stream - downstream (*Canariega bridge*)	0.0734 [0.2860]	0.0325 [0.2030]	0.2020† [0.5195]	0.0564 [0.2849]
Partido stream – upstream (*Azud de la Matanza*)	0.0956 [0.4455]	0.0472 [0.3299]	0.6685† [0.3684]	0.1089†† [0.4035]
Partido stream – downstream (*Ajolí bridge*)	0.0727 [0.0971]	0.0902 [0.0356]	0.7859† [0.2042]	0.1770†† [0.2787]

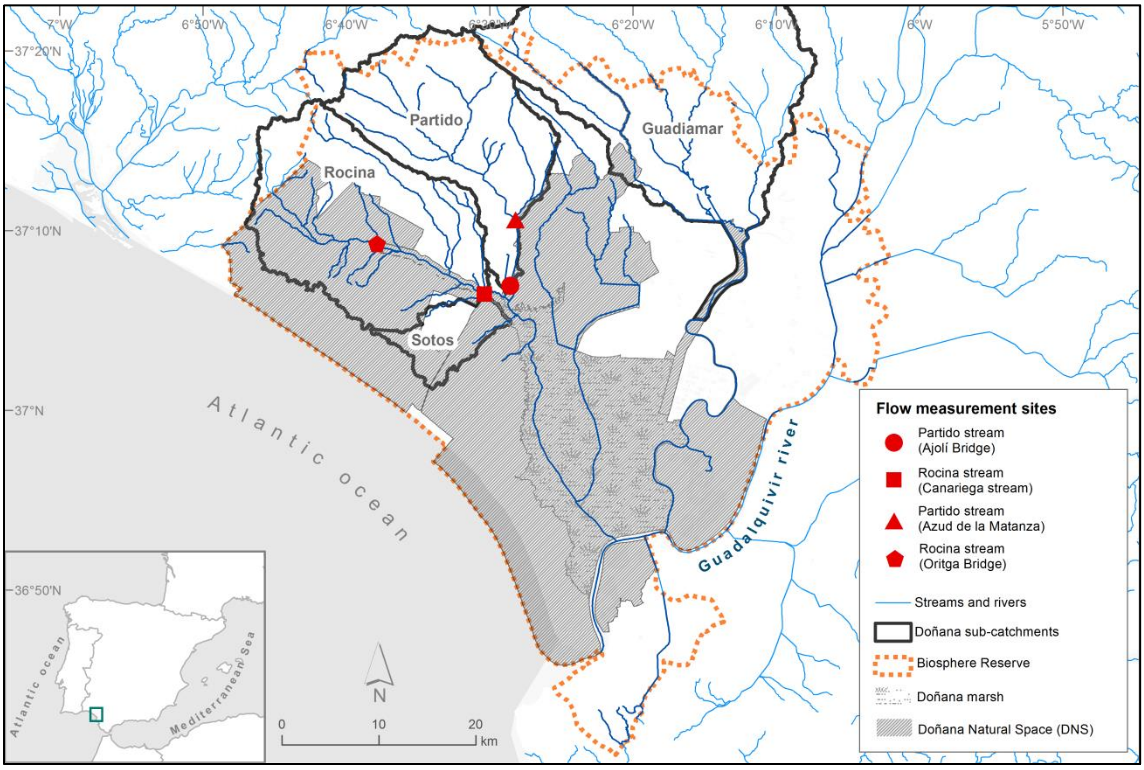

Table S4. Reference and limit values described in the Spanish Royal Decree 817/2015 for assessing the ecological status of the WFD waterbody types included within this study (R-T02, R-T18 and L-T25). Note that for type L-T25 (Marsh, Guadiamar and Soto Grande stream) there are not limit values for any nutrient species.

Waterbody	WFD code (Spain)	Indicator	Units	Reference conditions	Limits for shifting status class			
					Very good/Good	Good/Moderate	Moderate/Poor	Poor/Bad
Partido stream	R-T02 (river)	IBMWP		90	0.89	0.54	0.32	0.13
		IMMi-T		1	0.826	0.682	0.455	0.227
		IPS		14	0.94	0.71	0.47	0.24
		QBR		65	0.833			
		pH			6.5-8.7	from 6 to 9		
		Oxygen	mg/L			5		
		% Oxygen	%		70-100	60-120		
		Amonium	mg NH_4/L		0.3	1		
		Phosphates	mg PO_4/L		0.2	0.4		
		Nitrates	mg NO_3/L		20	25		
Rocina stream/Soto Chico stream	R-T18 (river)	IBMWP		78	0.82	0.5	0.29	0.13
		IMMi-T		1	0.844	0.696	0.464	0.232
		IPS		14	0.98	0.74	0.64	0.24
		QBR		60	0.833			
		pH			6.5-8.7	from 6 to 9		
		Oxygen	mg/L			5		
		% Oxygen	%		70-100	60-120		
		Amonium	mg NH_4/L		0.2	0.6		
		Phosphates	mg PO_4/L		0.4	0.5		
		Nitrates	mg NO_3/L		10	25		
Marsh/Guadiamar /Soto Grande stream	L-T25 (lake)	IBCAEL		6.19	0.78	0.59	0.39	0.2
		Macrophyte richness	Nº species	23		0.48	0.27	0.1
		Eutrophic macrophyte cover	%	0	0.99	0.9	0.5	0.5
		Exotic macrophyte cover	%	0	1	0.95	0.75	0.5
		Helophyte cover	%	80	0.88	0.75	0.37	0.13
		Hydrophyte cover	%	90	0.83	0.55	0.28	0.01
		pH				(7.5-10)	(≤7.5-≥10)	

Methods S1. Remote sensing of greenhouse expansion

From each hydrological year (24 in total) we selected one cloud-free Landsat image from autumn and another from spring (48 images in total). For each year, we grouped both autumn and spring images into a single 12-band image (B1: Blue, autumn; B2: Green, autumn; B3: Red, autumn; B4: NIR, autumn; B5: SWIR1, autumn; B6: SWIR2, autumn; B7: Blue, spring; B8: Green, spring; B9: Red, spring; B10: NIR, spring; B11: SWIR1, spring; B12: SWIR2, spring). For each image, we identified and classified different land covers such as greenhouses, urban areas, forested areas and other crops by simultaneously applying eight automatic target detection methods: Matched Filtering (MF) [2], Constrained Energy Minimization (CEM) [3], Adaptive Coherence Estimator (ACE) [4], Spectral Angle Mapper (SAM) [5], Orthogonal Subspace Projection (OSP) [6], Target-Constrained Interference-Minimized Filter (TCIMF) [7], Mixture Tuned Target-Constrained Interference-Minimized Filter (MTTCIMF) [8], and Mixture Tuned Matched Filtering (MTMF) [9]. Afterwards, we used two filtering options (i.e. clumping and sieving) to clean up misdetected pixels and false positives in the category of "greenhouses". To check the quality of performance of the classification methods, we used the image corresponding to the 2013 hydrological year. We randomly distributed 1,200 points within the area classified as "greenhouse" and used an orthophoto from April 2013 (corresponding to the peak production season for greenhouse crops) to check whether these points fell in or out the real area covered by greenhouses. This work was carried out at the Remote Sensing Lab (LAST) at the Doñana Biological Station (EBD-CSIC, Seville).

References

[1] Díaz-delgado R, D Aragonés, I Afán, J Bustamante, 2016. Long-Term Monitoring of the Flooding Regime and Hydroperiod of Doñana Marshes with Landsat Time Series (1974–2014) Remote Sens. 2016, 8, 775; doi:10.3390/rs8090775

[2] Chen, J. Y. and I. S. Reed, 1987, A detection algorithm for optical targets in clutter, *IEEE Trans. on Aerosp. Electron. Syst.*, V. AES-23, No. 1.

[3] C.-I Chang, J.-M. Liu, B.-C. Chieu, C.-M. Wang, C. S. Lo, P.-C. Chung, H. Ren, C.-W. Yang, and D.-J. Ma, 2000.“A generalized constrained energy minimization approach to subpixel target detection for multispectral imagery,” Optical Engineering, vol. 39, no. 5, pp. 1275-1281.

[4] S. Kraut, L. L. Scharf, and R. W. Butler, 2005. “The adaptive coherence estimator: a uniformly most-powerful-invariant adaptive detection statistic,” IEEE Trans. on Signal Processing, vol. 53, no. 2, pp. 427-438

[5] Kruse, F. A., Lefkoff, A. B., Boardman, J. B., Heidebrecht, K. B., Shapiro, A. T., Barloon, P. J., and Goetz, A. F. H., 1993, The Spectral Image Processing System (SIPS) - Interactive Visualization and Analysis of Imaging Spectrometer Data: *Remote Sensing of Environment*, Special issue on AVIRIS, May-June 1993, v. 44, pp. 145 - 163.

[6] J. C. Harsanyi and C.-I Chang, 1994. “Hyperspectral image classification and dimensionality reduction: an orthogonal subspace projection approach,” IEEE Trans. On Geoscience and Remote Sensing, vol. 32, no. 4, pp. 779-785,

[7] H. Ren and C.-I Chang, 2000. “Target-constrained interference-minimized approach to subpixel target detection for hyperspectral imagery,” Optical Engineering, vol. 39, no. 12, pp. 3138-3145.

[8] X. Jin, S. Paswaters, and H. Cline, 2009. "A comparative study of target detection algorithms for hyperspectral imagery," In Algorithms and Technologies for Multispectral, Hyperspectral, and Ultraspectral Imagery XV. Proceedings of SPIE, Vol. 7334, pp. 73341W1-73341W12.

[9] J. W. Boardman, 1998. "Leveraging the high dimensionality of AVIRIS data for improved sub-pixel target unmixing and rejection of false positives: mixture tuned matched filtering," In: 7th JPL Airborne Geoscience Workshop, pp. 55-56.